



HAL
open science

Hand Magnets and the Destruction of Ancient Meteorite Magnetism

Foteini Vervelidou, Benjamin Weiss, France Lagroix

► **To cite this version:**

Foteini Vervelidou, Benjamin Weiss, France Lagroix. Hand Magnets and the Destruction of Ancient Meteorite Magnetism. *Journal of Geophysical Research. Planets*, 2023, 128 (4), 10.1029/2022JE007464 . insu-04149357

HAL Id: insu-04149357

<https://insu.hal.science/insu-04149357>

Submitted on 4 Jul 2023

HAL is a multi-disciplinary open access archive for the deposit and dissemination of scientific research documents, whether they are published or not. The documents may come from teaching and research institutions in France or abroad, or from public or private research centers.

L'archive ouverte pluridisciplinaire **HAL**, est destinée au dépôt et à la diffusion de documents scientifiques de niveau recherche, publiés ou non, émanant des établissements d'enseignement et de recherche français ou étrangers, des laboratoires publics ou privés.



Distributed under a Creative Commons Attribution 4.0 International License

Hand Magnets and the Destruction of Ancient Meteorite Magnetism



Key Points:

- The magnetic records of meteorites provide information about planetary formation and evolution, yet they are routinely destroyed by magnets
- We demonstrate the effect of magnets numerically, experimentally, and through a paleomagnetic study of the Martian meteorite Northwest Africa 7034
- We recommend the use of susceptibility meters for meteorite identification as a nondestructive and more accurate identification technique

Supporting Information:

Supporting Information may be found in the online version of this article.

Correspondence to:

F. Vervelidou,
foteini@mit.edu

Citation:

Vervelidou, F., Weiss, B. P., & Lagroix, F. (2023). Hand magnets and the destruction of ancient meteorite magnetism. *Journal of Geophysical Research: Planets*, 128, e2022JE007464. <https://doi.org/10.1029/2022JE007464>

Received 20 JUL 2022
Accepted 3 APR 2023

Foteini Vervelidou^{1,2} , Benjamin P. Weiss¹ , and France Lagroix² 

¹Department of Earth, Atmospheric and Planetary Sciences, Massachusetts Institute of Technology, Cambridge, MA, USA, ²CNRS, Institut de Physique du Globe de Paris, Université Paris Cité, Paris, France

Abstract Meteorites provide invaluable records of planetary formation and evolution. Studies of their paleomagnetism have constrained accretion in the protoplanetary disk, the thermal evolution and differentiation of planetesimals, and the history of planetary dynamos. Yet, the potential of these magnetic records in advancing the field of planetary science is severely hindered by a widely used technique: application of hand magnets to assist in meteorite classification. Touching a meteorite with a magnet results in near-instantaneous destruction of its magnetic record. Here, we showcase the destructive effects of exposing meteorites to magnets through numerical modeling, a controlled remagnetization experiment on a terrestrial basalt, and a paleomagnetic study of the oldest known Martian meteorite, the Northwest Africa (NWA) 7034 pairing group. NWA 7034 is a polymict regolith breccia containing zircon crystals with crystallization ages older than 4.4 billion years. As such it contains materials that are sufficiently old to have formed during the time Mars is most likely to have had a core dynamo. Unfortunately, we found that all nine paired stones of NWA 7034 that we investigated were remagnetized by hand magnets, as has been observed for many other hot desert meteorites. We recommend that magnets not be applied to meteorites during collection and curation. Instead, a low-field susceptibility meter is a far more sensitive and completely nondestructive tool for meteorite classification.

Plain Language Summary Meteorites are objects that originate from a celestial body other than Earth, such as other planets, the Moon, asteroids, and comets. They were ejected from their parent bodies following a collision or an impact and later landed on Earth. The remanent magnetization of meteorites provides invaluable information about how planets formed and evolved. Unfortunately these ancient magnetic records are commonly destroyed soon after the meteorites are discovered due to a widely used classification technique: touching them with strong magnets. Here, we present the results of a computer modeling, an experiment in which a rock is exposed to a hand magnet, and a magnetic study of the oldest known Martian meteorite, Northwest Africa (NWA) 7034. NWA 7034 has crystals that are older than 4.4 billion years old and date from the time when Mars had an internally generated magnetic field. As such, the study of NWA 7034's magnetic record has the potential to provide valuable insights about the Martian magnetic field and consequently about the geological and climatological evolution of Mars. However, we show that its magnetic record has been destroyed by hand magnets. We suggest that susceptibility-meters be used instead because they are nondestructive and a more accurate identification technique.

1. Introduction

The tens of thousands of known meteorites are thought to be samples of more than 100 parent bodies including asteroids, the Moon, and Mars (Weisberg et al., 2006). They provide unique records of planet formation and evolution, including evolution of the protoplanetary disk, planetary accretion, and planetary thermal evolution and differentiation.

The study of the more than 200 known Martian meteorites, our only rock samples from Mars (Udry et al., 2020), has significantly advanced our understanding of the geochemical and geophysical evolution of the Red Planet. Yet, only for a small subset of them has it been possible to study their preterrestrial natural remanent magnetization (NRM) (Rochette et al., 2001), the semipermanent alignment of electron spins that provides a record of exposure to past magnetic fields on Mars.

Mars currently does not possess a global, internally generated, magnetic field, but regions of its crust are strongly magnetized (Johnson et al., 2020; Langlais et al., 2019; Morschhauser et al., 2018). This indicates that Mars once had a global dynamo field powered by its convecting metallic core, which may have ceased

© 2023. The Authors.

This is an open access article under the terms of the [Creative Commons Attribution License](https://creativecommons.org/licenses/by/4.0/), which permits use, distribution and reproduction in any medium, provided the original work is properly cited.

after 3.7 billion years (Ga) ago (Mittelholz et al., 2020). Amongst all currently known Martian meteorites, only two contain materials with crystallization ages older than 4 billion years old. All other Martian meteorites postdate by billions of years the likely shutdown time of the Martian dynamo and therefore can only retain records of crustal remanent magnetic fields (Nyquist et al., 2001). The two exceptions are Allan Hills 84001, an orthopyroxenite with a crystallization age of approximately 4.1 Ga (Weiss et al., 2008) and the Northwest Africa (NWA) 7034 pairing group (hereafter, NWA 7034), a polymict breccia with zircon and baddeleyite crystals with U-Pb crystallization ages older than 4.4 billion years (Bouvier et al., 2018; Cassata et al., 2018; McCubbin et al., 2016). As such, NWA 7034 is the only known meteorite to be sufficiently old that we have confidence should have acquired a direct record of the Martian core dynamo. Access to this record could provide unique constraints on the strength, timing, and evolution of the Martian dynamo, and by implication, on the composition and thermal state of Mars' deep interior. Furthermore, measurements of the field's paleointensity could test the hypothesis that Mars' thick ancient atmosphere was once protected from loss by a strong ($> \sim 50 \mu\text{T}$) dynamo field (Lundin et al., 2007; Sakata et al., 2020). Two other exceptional aspects of this meteorite are that it is just one of four known Martian meteorites with sufficient concentrations of magnetic minerals to account for the strong crustal magnetic fields (Gattacceca et al., 2014), and the only meteorite whose composition matches the estimated composition of the average Martian crust (Agee et al., 2013).

However, no study has been able to investigate the ancient magnetic record of this meteorite. Gattacceca et al. (2014) found that the NRMs of NWA 7034 and one of its paired stones, NWA 7533, have been completely overprinted by magnets. The use of magnets as an identification technique is widespread among meteorite hunters and collectors, particularly when assessing meteorites found in hot deserts (Gattacceca & Rochette, 2004; Rochette et al., 2001; Wasilewski & Dickinson, 2000; Weiss et al., 2010). Magnets have been used by meteorite hunters of the National Science Foundation (NSF)-funded Antarctic Search for Meteorites (ANSMET) program to assess samples whose classification was deemed ambiguous after visual inspection (Harvey et al., 2014; Love, 2013) but this practice has by now been largely, albeit not completely, abandoned. Even falls (i.e., meteorites whose fall from space on Earth is observed), sometimes get exposed to strong hand magnets (Bischoff et al., 2021). This is unfortunate because magnets can help identify only the subset of meteorites that is rich in iron-nickel metal, which is what makes them more strongly attracted to magnets relative to most terrestrial crustal rocks. Other than iron and stony iron meteorites, this subset is mostly comprised of ordinary chondrites, which tend to be among the least valuable meteorite groups. Many of the most rare and valuable meteorites, including most Martian meteorites, are poor in magnetic minerals and therefore cannot be easily distinguished from terrestrial rocks with a magnet. The use of magnets as a meteorite identification technique is therefore not only detrimental but also inefficient.

Magnets commonly used for meteorite identification are rare-earth magnets (i.e., composed of neodymium or samarium-cobalt), with typical pull forces of tens of kg (e.g., MeteoriteMen, 2022), which correspond to typical surface magnetic fields between 0.3 and 0.7 T, typical sizes of a few centimeters, and typical grades between N42 to N52 (e.g., K & J Magnetics, Inc, 2023; Weir et al., 2020). Unfortunately, given that the magnetic carriers in meteorites are dominantly kamacite, magnetite, and pyrrhotite, which mainly form grains that will be remagnetized by exposure to fields of $< 0.3 \text{ T}$, exposing most meteorites to such a strong magnetic field results in the near-instantaneous (on the order of ns) erasure of their magnetic record. As a result, the vast majority of hot desert meteorites that have been studied paleomagnetically have been found to be predominantly or completely remagnetized by magnets (Gattacceca & Rochette, 2004; Rochette et al., 2001; Weiss et al., 2010).

The widespread use of this identification technique severely impacts the ability of meteorite paleomagnetism to address planetary science questions. With this study, we aim at raising awareness on this issue within the broader planetary science community as a first step toward enacting change: abandoning the technique of touching or approaching meteorites with magnets in favor of well-established, nondestructive, and more accurate identification techniques like the use of portable susceptibility-meters. In Section 2, we estimate numerically the remagnetization effect of magnets. In Section 3, we perform a controlled remagnetization experiment on a terrestrial basalt, which allows us to test the calculations of Section 2. In Section 4, we report our study of the paleomagnetism of hot desert Martian meteorite NWA 7034 pairing group. In Section 5, we discuss the use of portable susceptibility-meters as an alternative identification technique. We provide a short summary of the main takeaways in Section 6.

2. Numerical Estimation of the Magnetic Effect of a Magnetized Prism

The magnetic field for a rectangular prism magnetized along the \hat{x} direction has been derived analytically by Yang et al. (1990). Camacho and Sosa (2013) adapted these results for a rectangular prism uniformly magnetized along the \hat{z} direction (see their Section 2.5). The MATLAB routine FieldBar.m by Cébron (2021) makes use of the results by Camacho and Sosa (2013) but corrects for an error in the equation of the magnetic field along the \hat{y} direction and an error in the calculation of the magnetic field inside the magnet (see the ReadMe file of Cébron (2021) for details). Accounting for these corrections, the magnetic field along the \hat{x} , \hat{y} , and \hat{z} directions of a rectangular prism uniformly magnetized along the \hat{z} direction is given by the following equations:

$$B_x(x, y, z, a, b, c) = \frac{\mu_0 M}{4\pi} \ln \frac{F_2(-x, y, -z, a, b, c) F_2(x, y, z, a, b, c)}{F_2(x, y, -z, a, b, c) F_2(-x, y, z, a, b, c)} \quad (1)$$

$$B_y(x, y, z, b, a, c) = \frac{\mu_0 M}{4\pi} \ln \frac{F_2(-y, x, -z, a, b, c) F_2(y, x, z, a, b, c)}{F_2(y, x, -z, a, b, c) F_2(-y, x, z, a, b, c)} \quad (2)$$

$$B_z(x, y, z, a, b, c) = \begin{cases} B_3(x, y, z, a, b, c), & (|x|, |y|, |z|) > (a, b, c) \\ B_3(x, y, z, a, b, c) + \mu_0 M, & (|x|, |y|, |z|) \leq (a, b, c) \end{cases}, \quad (3)$$

where

$$B_3(x, y, z, a, b, c) = -\frac{\mu_0 M}{4\pi} [F_1(-x, y, z, a, b, c) + F_1(-x, y, -z, a, b, c) + F_1(-x, -y, z, a, b, c) + F_1(-x, -y, -z, a, b, c) + F_1(x, y, z, a, b, c) + F_1(x, y, -z, a, b, c) + F_1(x, -y, z, a, b, c) + F_1(x, -y, -z, a, b, c)] \quad (4)$$

$$F_1(x, y, z, a, b, c) = \arctan \frac{(x+a)(y+b)}{(z+c)\sqrt{(x+a)^2 + (y+b)^2 + (z+c)^2}} \quad (5)$$

$$F_2(x, y, z, a, b, c) = \frac{\sqrt{(x+a)^2 + (y-b)^2 + (z+c)^2} + b - y}{\sqrt{(x+a)^2 + (y+b)^2 + (z+c)^2} - b - y}, \quad (6)$$

where x , y , and z are the distance of the observation point from the magnet's center along the \hat{x} , \hat{y} , and \hat{z} directions, respectively, μ_0 is the permeability of free space, M is the magnetization of the prism, and $a = L_x/2$, $b = L_y/2$, and $c = L_z/2$, with L_x , L_y , and L_z the dimensions of the prism in the \hat{x} , \hat{y} , and \hat{z} directions, respectively.

We used FieldBar.m by Cébron (2021) to calculate the magnetic field surrounding typical hand magnets and their effect on rocks of various sizes. In particular, we considered the cases of three grade N52 neodymium bar magnets of size $L_x = 4$ cm, $L_y = 4$ cm, and $L_z = 2$ cm that are permanently magnetized along \hat{z} , with 0.3, 0.5, and 0.7 T surface polar fields. The magnetic field surrounding the 0.5 T magnet, plotted on the y - z plane, is shown in Figure 1a. According to this figure, any rock brought within 3 magnet radii of such a magnet will be exposed to magnetic fields in excess of 50 mT.

Figure 1b shows the volume fraction of a rock that exceeds a certain magnetic field intensity when placed at the pole of a bar magnet with the same dimensions as in Figure 1a, assuming magnets of different strength. Here, we used FieldBar.m to calculate the magnetic field in the three dimensional space around the magnet. According to this figure, a 10 g rock will be exposed to 100 mT over its entire volume when touched by a hand magnet with a 0.3 T polar surface field and therefore all magnetic grains with <100 mT coercivity will be fully remagnetized (coercivity is the magnetic field intensity required to remagnetize a given magnetic grain). It requires a >100 g rock for such a magnet to expose <40% of the rock's volume to 100 mT, but even such a large rock will have 80% of its volume exposed to 100 mT when touched by a hand magnet with a 0.7 T polar surface field.

We will now test these results with an experiment in which we expose a basalt to a magnet. We will use Equation 3 to assess the volume fraction of the rock that has experienced a given peak field and the intensity of remagnetization as a function of the position in the rock, and we will compare these results to our measurements.

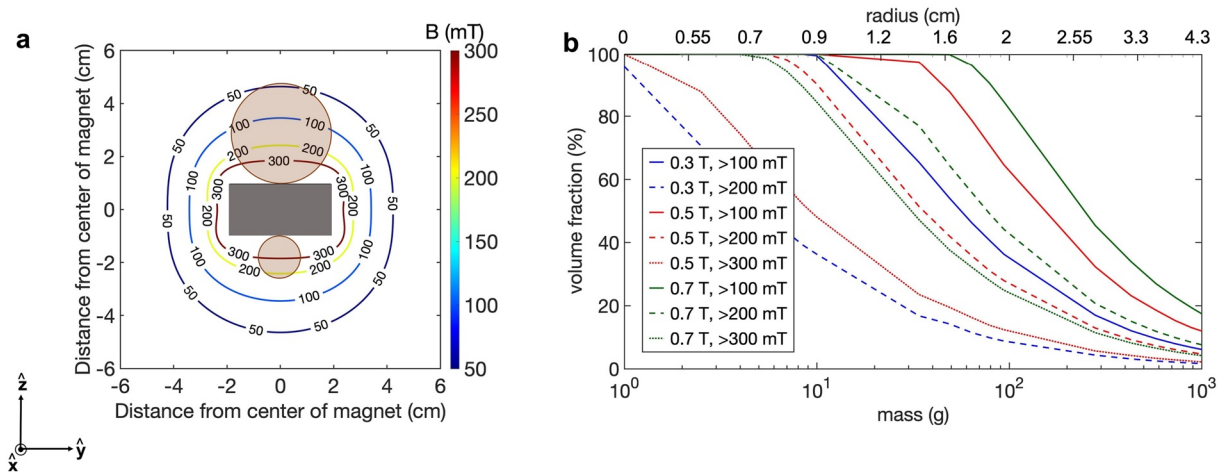


Figure 1. The magnetic field of a neodymium bar magnet and its effect on rock samples. (a) The intensity of the magnetic field of a bar magnet (gray), with magnetization along \hat{z} , a polar surface field of 0.5 T, and dimensions $L_x = 4$ cm, $L_y = 4$ cm, and $L_z = 2$ cm, is shown on the y - z plane at $x = 0$, as a function of the distance from the magnet's center located at $x = y = z = 0$. The brown circles at the north and south poles of the bar magnet represent the cross-sectional areas of rocks with masses of 80 and 6 g, respectively. (b) The volume fraction of a rock that experiences >100 , >200 , and >300 mT fields (solid, dashed, and dotted line, respectively) when placed at the pole of the bar magnet with the same dimensions as in (a), assuming 0.3, 0.5, and 0.7 T polar surface fields (blue, red, and green lines, respectively). Results shown as a function of the rock's mass (lower abscissa) and radius (upper abscissa). A spherical shape and density of 3 g cm^{-3} is assumed for the rocks.

3. Experimental Estimation of the Effect of a Hand Magnet on Rock Samples

The goal of this experiment is to study the effect of a hand magnet on rock samples and to subsequently establish criteria for identifying samples exposed to magnets. This builds on an experiment conducted by Wasilewski and Dickinson (2000), in which the demagnetization curve of the NRM of the Bjürbole meteorite was compared with its demagnetization curve after the same material had been touched by a hand magnet. Here, we focus on the effect of magnets on the NRM intensity and direction of basaltic rock samples as a function of distance from the magnet. We examine these effects as a function of the strength of the applied magnetic fields.

The rock sample for this experiment is a $4 \times 3 \times 0.5$ cm piece, cut from sample 22SM-53, a subaerial massive basalt, collected from the São Miguel Island in the Azores with an age of 800 ky (Ricci et al., 2020). Its hysteresis loop, obtained using a PMC MicromagTM 3900 Vibrating Sample Magnetometer at the Institut de Physique du Globe de Paris (IPGP) Paleomagnetism Laboratory, is shown in Figure 3. According to these measurements, the sample has a mean pseudo-single domain grain size ($H_{cr}/H_c = 2.01$ and $M_{rs}/M_s = 0.225$, with H_{cr} the coercivity of remanence, H_c the coercivity, M_{rs} the saturation remanent magnetization, and M_s the saturation magnetization) and a maximum coercivity of 300 mT. This sample has been subdivided into 14 specimens with 13 of these specimens, each approximately 0.5 cm^3 in size, exposed to cycles of demagnetization and remagnetization (see Figure 2 for the specimens' configuration and Table S1 in Supporting Information S1 for their masses). For this and the respective magnetization measurements, we used an ASC D-2000T alternating field (AF) demagnetizer, a MMPM10 pulse magnetizer, a 2G Enterprises Superconducting Rock Magnetometer (SRM), and an AGICO JR-6 spinner magnetometer at the IPGP Paleomagnetism Laboratory. In particular, all 13 specimens underwent the following steps:

1. Three-axis AF demagnetization (i.e., exposure to an AC field with decreasing amplitude) with peak field at 200 mT.
2. Application of anhysteretic remanent magnetization (ARM) of 200 mT peak AF and 0.1 mT bias DC field along \hat{x} .
3. Stepwise AF demagnetization along \hat{x} , with 10 mT steps, up to 100 mT.
4. Application of ARM of 200 mT peak AF and 0.1 mT bias DC field along \hat{x} .
5. Exposure to the magnetic field of a $4 \times 4 \times 2$ cm N40 neodymium magnet, magnetized along \hat{z} , with a polar surface field of 0.4 T. This produced an isothermal remanent magnetization (IRM) (i.e., magnetization from exposure to a strong field at room temperature). The placement of the magnet with respect to the rock specimens is shown in Figure 2. The magnet was then removed along \hat{x} .

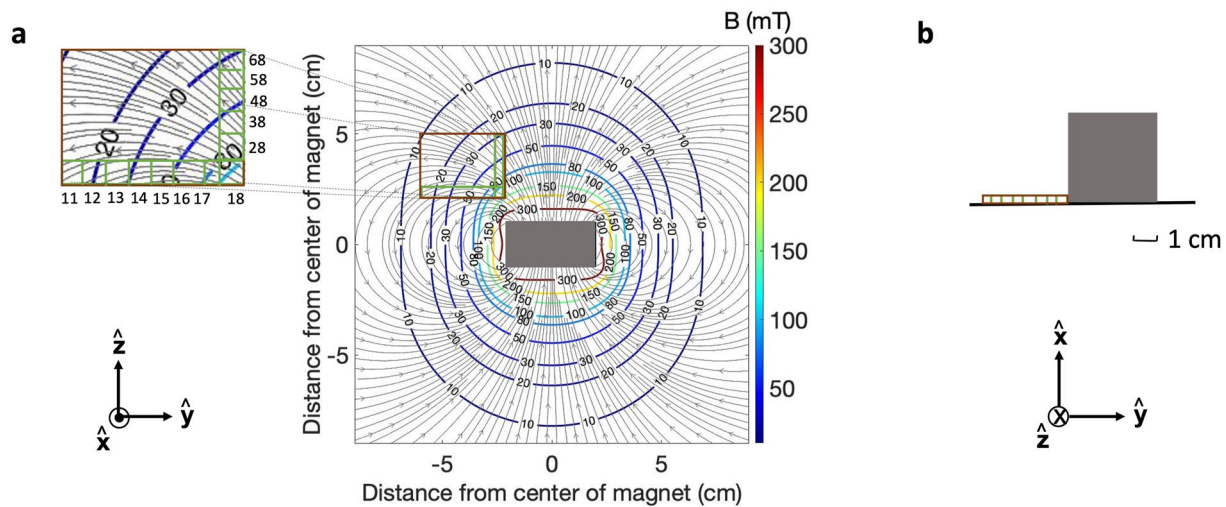


Figure 2. Setup for the controlled remagnetization experiment. (a) The magnetic field of the N40 neodymium magnet, with magnetization along \hat{z} , a polar surface field of 0.4 T, and dimensions $L_x = 4$ cm, $L_y = 4$ cm, $L_z = 2$ cm, is shown on the y - z plane at $x = -0.75$ cm, as a function of the distance from the magnet's center, located at ($x = y = z = 0$). Superimposed to the intensity contour lines (colored lines) are the magnetic field lines (gray). The projection of the $L_x = 0.5$ cm, $L_y = 4$ cm, $L_z = 3$ cm rock sample, whose center lies at ($x = -0.75$ cm, $y = -4$ cm, $z = 3.5$ cm), is shown in red. The 13 specimens were obtained from the bottom and right-hand sides of the sample, shown in green. The inset shows the exact location of each specimen (11–18 and 28–68) and a denser version of the magnetic field lines. The coordinate system is shown at the bottom left. (b) The magnet (gray) and the rock sample (red) viewed from a different perspective (coordinate system shown at the bottom).

6. Stepwise three-axis AF demagnetization, with 5 mT steps up to 30 mT, and then 10 mT steps up to 100 mT.
7. Application of a saturation IRM (sIRM) of 1 T, along the \hat{z} direction.
8. Stepwise AF demagnetization along \hat{z} , with 5 mT steps up to 30 mT, and then 10 mT steps up to 100 mT (same step-wise demagnetization protocol as at step 6).

Steps 1–4 and 6–8 were each conducted on individual specimens after removal from their original locations in the rock, whereas step 5 occurred after temporarily reassembling all the specimens back into their original positions.

Steps 1–3 have the goal of studying how the specimens would demagnetize if they carried a thermoremanent magnetization (TRM), given that ARM is a laboratory analog of TRM (Yu et al., 2003). The intensity of the specimens' ARM during the AF demagnetization is given in Figure 4 as a function of the AF demagnetization

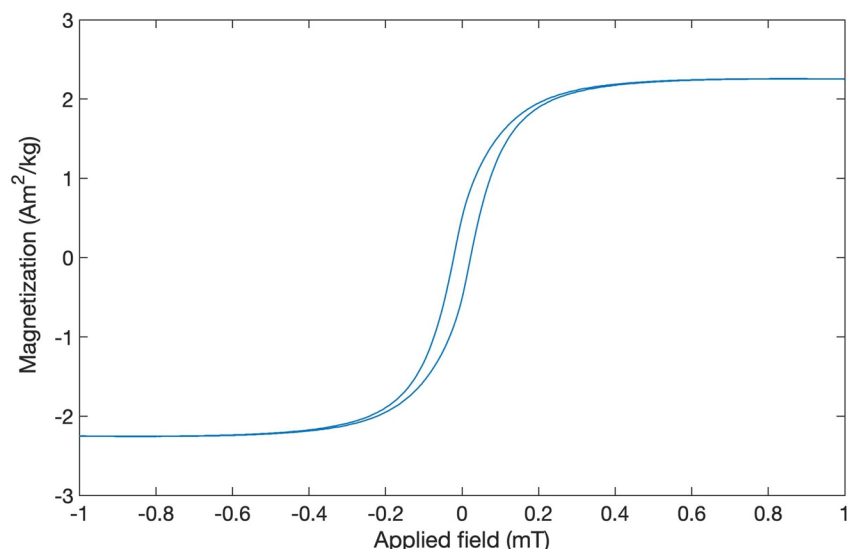


Figure 3. Hysteresis loop of the 22SM-53 basalt sample used in the remagnetization experiment. Shown is the mass-normalized magnetic moment as a function of the applied field, after high-field paramagnetic slope correction.

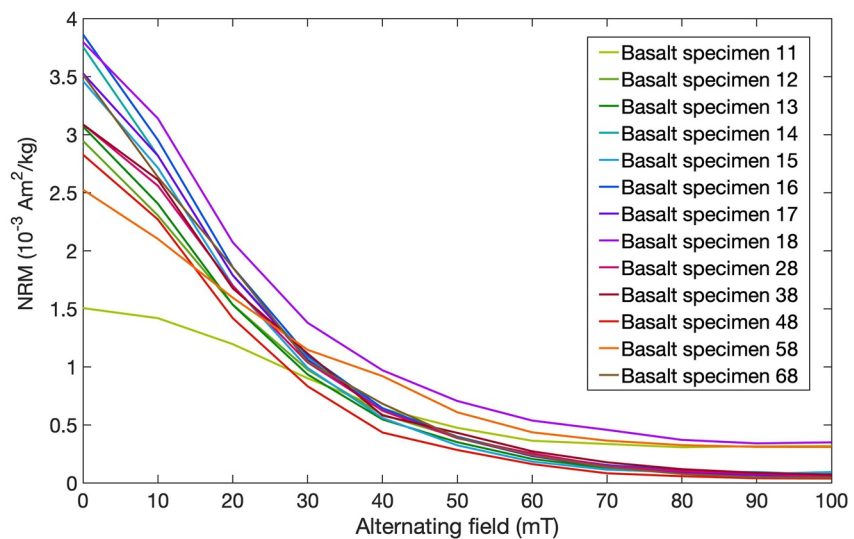


Figure 4. Alternating field (AF) demagnetization of anhysteretic remanent magnetization (ARM) of the 13 basalt specimens. The intensity of ARM with 200 mT peak AF and 0.1 mT bias DC field along \hat{x} , during single-axis AF demagnetization, as a function of AF step, for each specimen.

step. We observe that specimens are 11, 18, and 58 are not fully demagnetized by the 100 mT AF step. This indicates that their coercivity is higher than that of the other specimens, such that their NRM was not completely removed by step 1 and therefore their magnetization beyond 80 mT is rather the vector sum of the residual NRM and the applied ARM.

Steps 4 and 5 represent the case in which a rock sample initially carrying a TRM is exposed to a hand magnet. The magnetization obtained after this step is a combination of IRM and possibly a residual TRM (this combination is hereafter referred to as “NRM”). Figure 5 shows the magnetic field intensity to which each specimen is expected to be exposed based on its proximity to the hand magnet, according to Equations 1–6. According to this figure, increasing specimen numbers from 11 to 18 are expected to be exposed to progressively stronger magnetic fields. This is as expected since specimen 11 lies the furthest away from the magnet and specimen 18 lies the closest to it. The results for specimens 28 to 68 are similar to the ones for specimens 17 to 13. This is confirmed experimentally according to Figure 6, which shows the acquired mass-normalized NRM of each specimen as a function of its distance from the magnet.

The purpose of Step 6 was to estimate the maximum coercivity of grains remagnetized by the magnet, for each specimen. Figures 7 and 8 show the ARM and NRM demagnetization plots of specimens 11, 12, 14, 15, 18, 48, 58, and 68 (squares and circles, respectively). We see that for specimen 11, both demagnetization curves merge after the 20 mT AF step, which means that the magnet overprint is removed by that AF level, in agreement with our numerical calculations shown in Figure 5. Note that the ARM for this specimen does not plot exactly along \hat{x} but is slightly shifted toward $-\hat{y}$ (deep blue square). This is because its high coercivity (as already discussed and demonstrated in Figure 4) led to nonnegligible residual TRM even after being demagnetized at 200 mT (step 1). Namely, its NRM was a combination of the applied ARM along \hat{x} and a TRM, predominantly along $-\hat{y}$, which was acquired in the Earth’s field when the rock formed. After the ARM and NRM demagnetization curves merged at AF step 20 mT, they progressively shifted toward $-\hat{y}$, until what was left was that high coercivity (>200 mT) residual TRM (yellow squares and circles).

The ARM of specimen 12, which was fully demagnetized by 100 mT according to Figure 4, points directly along \hat{x} , as shown in Figure 7b (deep blue square). Its NRM demagnetization curve progressively approaches its ARM direction, moving from $-\hat{y}$ to \hat{x} , but the two curves do not fully merge. The NRM demagnetization curve of specimen 14 (shown in Figure 7c), moves toward its ARM curve but remains closer to $-\hat{y}$ than to \hat{x} .

Specimens 15–18 and 28–48 are fully remagnetized by the magnet (i.e., they are fully demagnetized without their magnetization direction ever approaching that of the ARM). Figures 7d, 8a, and 8b show the demagnetization curves for specimens 15, 18, and 48, respectively. This result is in agreement with Figure 5, which shows that

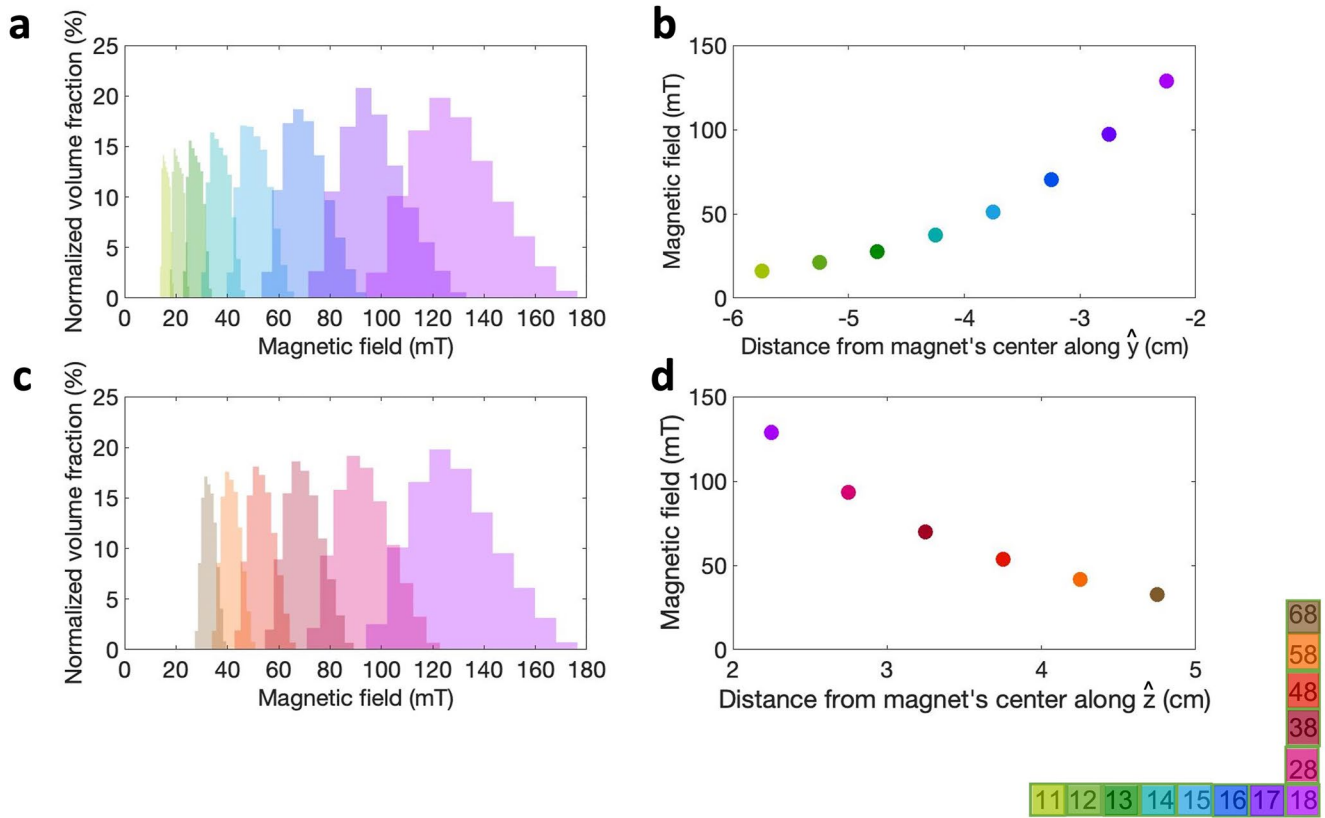


Figure 5. Calculated magnetic field intensity of the magnet shown in Figure 2 at the location of each basalt specimen. (a) Histograms of the normalized volume fraction of each specimen exposed to a given magnetic field intensity for specimens 11–18. (b) The mean intensity for specimens 11–18 as a function of the distance from the magnet's center along \hat{y} . (c) Histograms of the normalized volume fraction of each specimen exposed to a given magnetic field intensity for specimens 18–68. (d) The mean intensity for specimens 18–68 as a function of the distance from the magnet's center along \hat{z} . The relative location of each specimen, along with the colorbar, is shown at the bottom right.

specimens 15–18 and 28–48 were expected to experience magnetic fields of at least 60 mT. This is the AF step at which these specimens had already lost 90% of their ARM according to Figure 4 and is therefore the coercivity of the vast majority of their magnetic carriers. Among these seven specimens, specimen 18 has the highest coercivity but is also the one that due to its location with respect to the magnet experienced the strongest fields, between 100 and 180 mT (see Figure S1 in Supporting Information S1 for its IRM acquisition curve). Note also that the demagnetization curves of specimens 15 and 18 are curved below 20 mT. This curvature, which is commonly observed for meteorites exposed to magnets (e.g., NWA 1068, Gattacceca & Rochette, 2004), is likely a manifestation of the temporally changing orientation of the magnetic field lines as the hand magnet is removed away from the rock sample (Gattacceca & Rochette, 2004; Weiss & Elkins-Tanton, 2013).

Finally, the NRM demagnetization curves of specimens 58 and 68, shown in Figures 8c and 8d, approach the respective ARM demagnetization curves and merge with them around AF step 40 mT. Like specimens 11 and 12, these specimens retained much of their NRM due to their distal locations from the magnet.

The results shown in Figures 7 and 8 are in agreement with Figure 9, which shows the intensity of the specimens' NRM during AF demagnetization. We observe that the different specimens lost most of their NRM at progressively higher AF steps, with specimen 11 doing so at 20 mT and specimen 18 above 90 mT. Given that the NRM is two orders of magnitude stronger than the respective ARM (compare Figure 9 with Figure 4), Figures 7–9 demonstrate that it is possible to remove a magnet overprint by means of AF demagnetization as long as there is a subset of magnetic carriers whose coercivities are higher than the strength of the applied magnetic field. This possibility has been occasionally observed for some meteorites (e.g., Acfer 333, Gattacceca & Rochette, 2004).

The stereoplots in Figures 7 and 8 depict also the mean direction of the magnetic field that each of these specimens are expected to be exposed to according to Figure 2. A perfect agreement between this magnetic field

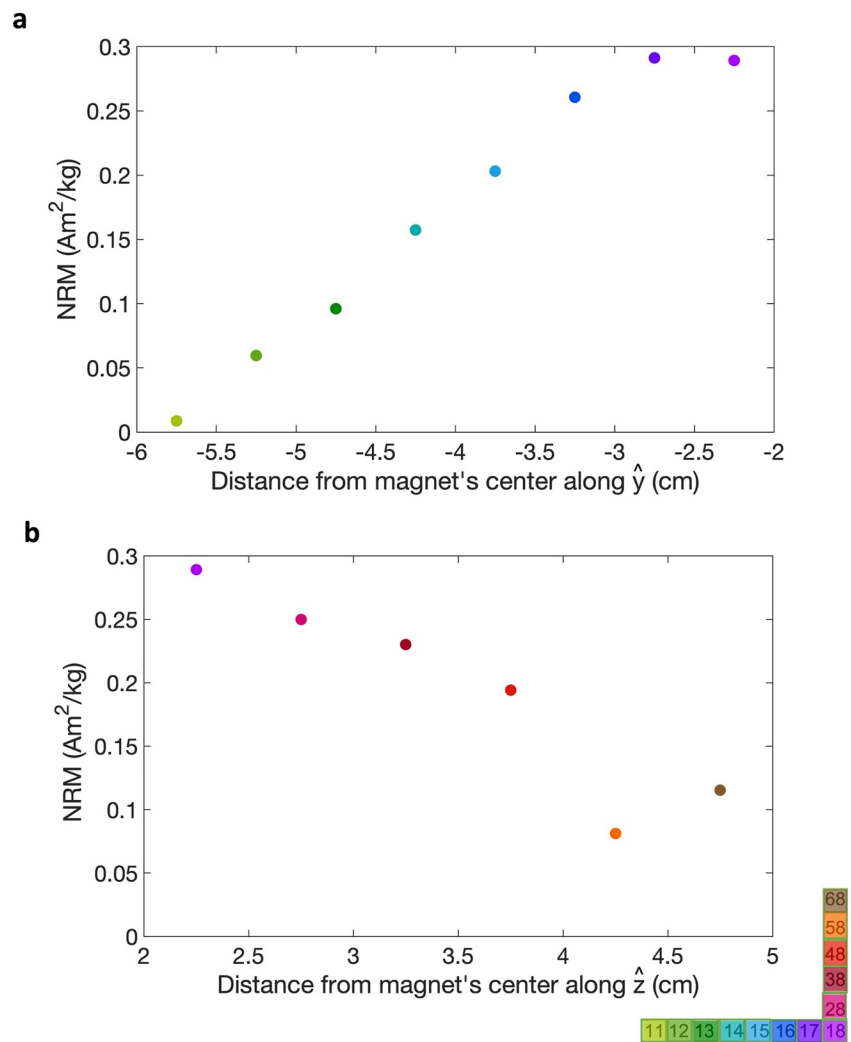


Figure 6. The intensity of the natural remanent magnetization of the 13 basalt specimens as a function of distance from the magnet. (a) Specimens 11–18, as a function of the distance from the magnet's center along \hat{y} (see Figure 2). (b) Specimens 18–68, as a function of the distance from the magnet's center along \hat{z} (see Figure 2). The relative location of each specimen, along with the colorbar, is shown at the bottom right.

direction (dark blue triangle) and that of the acquired magnetization (dark blue circle) is not expected as the effect of removing the magnet, which exposes the specimens to a time-varying field, is not taken into account. Even so, we observe very good agreement for all specimens. We expect the horizontal direction to be toward $-\hat{y}/-\hat{z}$ for specimens 11, 12, and 14, toward $-\hat{y}$ for specimen 15, and toward $-\hat{y}/\hat{z}$ for specimens 18, 48, 58, and 68, which is what we see. The vertical component is expected to be along $-\hat{x}$ for all specimens, which is as observed.

The purpose of the final steps of the measurement protocol, steps 7 and 8, was to estimate the strength of the field that magnetized the rock. This can be estimated from the ratio of NRM to sIRM prior to any demagnetization (a ratio known as the REM value, Wasilewski and Dickinson, 2000). Alternatively, for a multicomponent NRM, the paleointensity of a given NRM component can be estimated from the ratio of ΔNRM to ΔsIRM over the respective AF range (this is known as the REM' value when calculated for each adjacent pair of AF steps, Gattacceca & Rochette, 2004). Here, we present results using the REM method and a variant of the REM' method, in which we integrate REM' over the characteristic component of the NRM (e.g., Weiss et al., 2008), hereafter called the integrated REM'. The characteristic component is the most stable part of the NRM and is identified by its property to trend linearly toward the origin during AF demagnetization. Both the REM and the integrated REM' values are proxies for the paleointensity of the magnetic field that gave rise to a magnetization. In particular, TRM

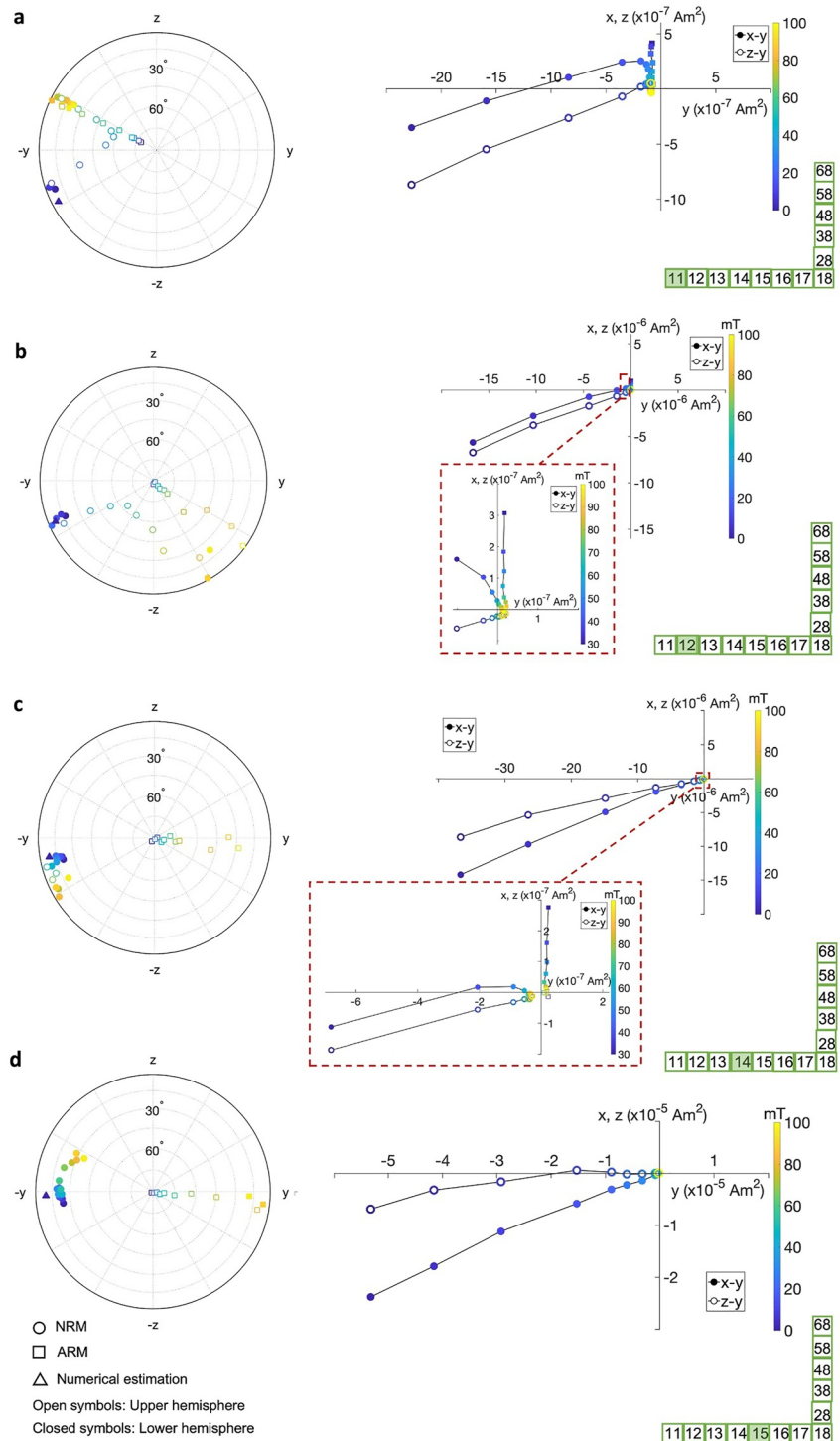


Figure 7. Anhyseretic remanent magnetization (ARM) and natural remanent magnetization (NRM) demagnetization of four basalt specimens. Shown are endpoints of the ARM and NRM vectors during progressive alternating field (AF) demagnetization, up to 100 mT. Closed and open symbols on the stereoplots represent endpoints on the lower ($x < 0$) and upper hemisphere ($x > 0$), respectively. Closed and open symbols on the orthographic projections of the NRM and ARM vectors represent endpoints onto the vertical ($y-z$) and horizontal ($y-x$) planes, respectively. Squares are used for the ARM and circles for the NRM. The triangles correspond to the direction of the magnetic field lines in Figure 2. The coordinate system is the one shown in Figure 2. (a) Specimen 11. (b) Specimen 12. Inset: AF demagnetization steps from 30 to 100 mT. (c) Specimen 14. Inset: AF demagnetization steps from 30 to 100 mT. (d) Specimen 15.

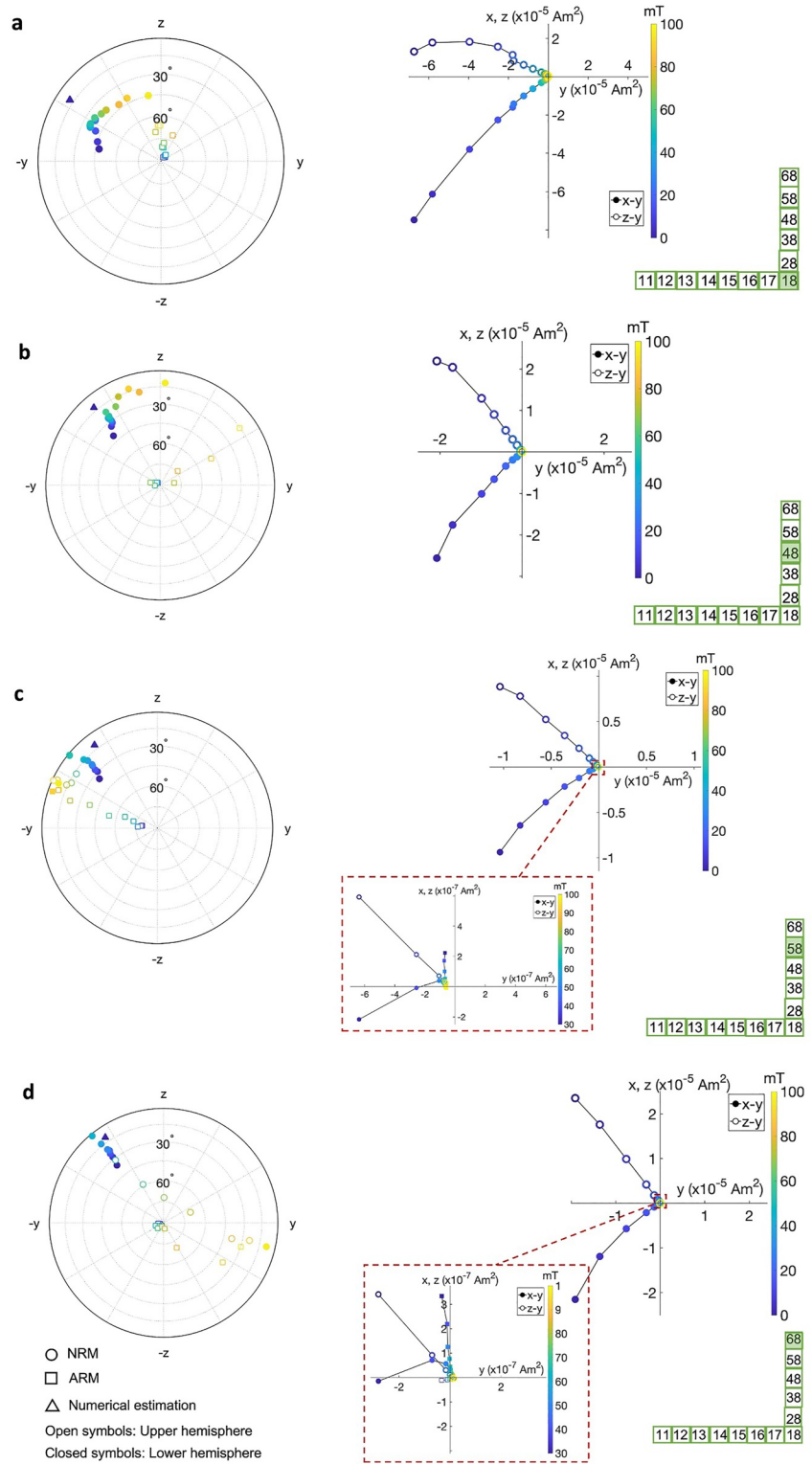


Figure 8. Same as Figure 7 but for different specimens. (a) Specimen 18, (b) Specimen 48. (c) Specimen 58. Inset: alternating field (AF) demagnetization steps from 30 to 100 mT. (d) Specimen 68. Inset: AF demagnetization steps from 30 to 100 mT.

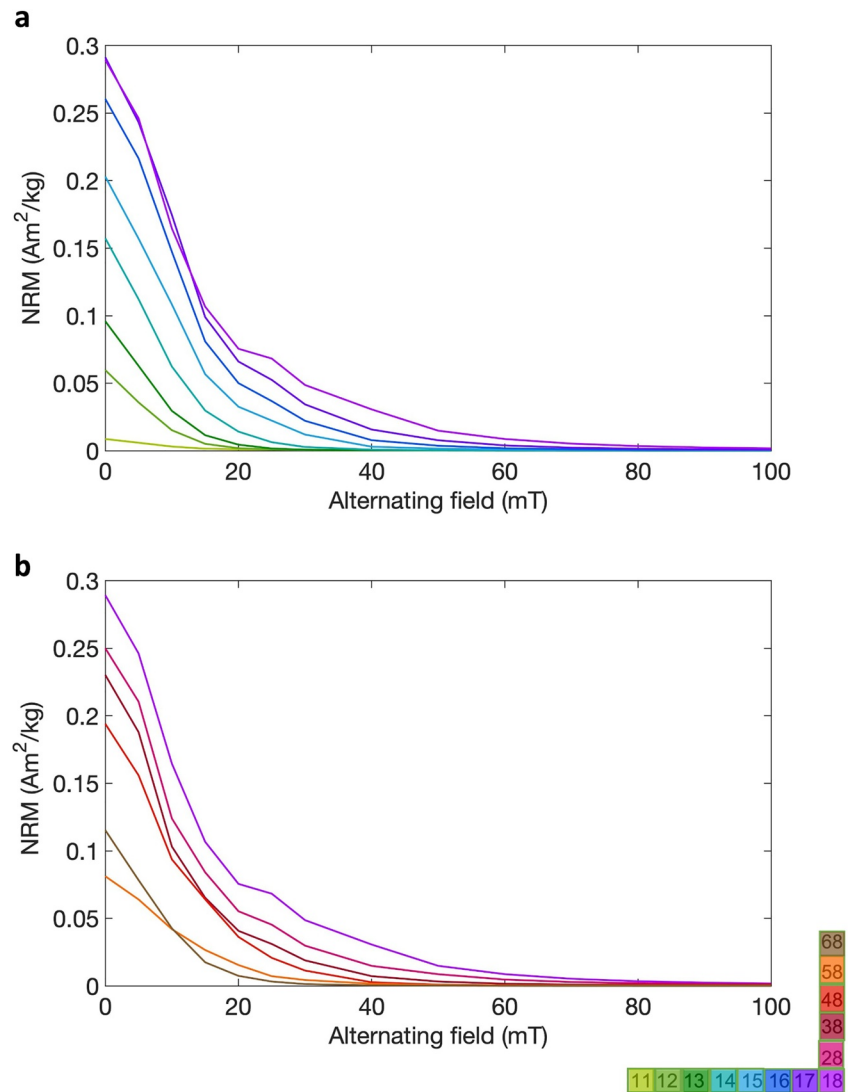


Figure 9. Natural remanent magnetization (NRM) demagnetization of the 13 basalt specimens. The intensity of NRM is shown as a function of the alternating field step. (a) For specimens 11–18. (b) For specimens 18–68. The relative location of each specimen, along with the colorbar, is shown at the bottom right.

acquired during cooling in the presence of a 50 μT magnetic field (and its ARM proxy acquired in bias field of comparable intensity) has an integrated REM' value of about 1.5% (Gattacceca & Rochette, 2004; Kletetschka et al., 2003).

Figure 10 shows the REM value of the ARM (green dots), the REM value of the NRM (blue dots), and the integrated REM' value of the NRM (red circles) for all specimens. We observe that the REM values of the ARM for all specimens are <1.5%. The integrated REM' values for the specimens that lie far enough from the magnet to have only experienced magnetic fields less than 60 mT are also <1.5%. For the remaining specimens (15–18, 28–48), precisely the ones that were fully remagnetized according to Figures 7 and 8, the integrated REM' values range from 30% to 70%. As expected, these values vary as a function of the specimen's distance from the magnet and are all lower than the respective REM values. The REM values for all specimens exceed 1.5%, ranging from 5% to 90% depending on the distance of the specimen from the magnet. The above results are in agreement with Gattacceca and Rochette (2004), who showed that the REM value is not an accurate paleointensity proxy in the case of multicomponent magnetization, and it is the REM' value that should be used instead. The fact that for specimens 11–14, 58, and 68 the integrated REM' value is below 1.5% is in agreement with Figures 7 and 8, which show that the NRMs of these specimens approach their ARM as AF demagnetization proceeds.

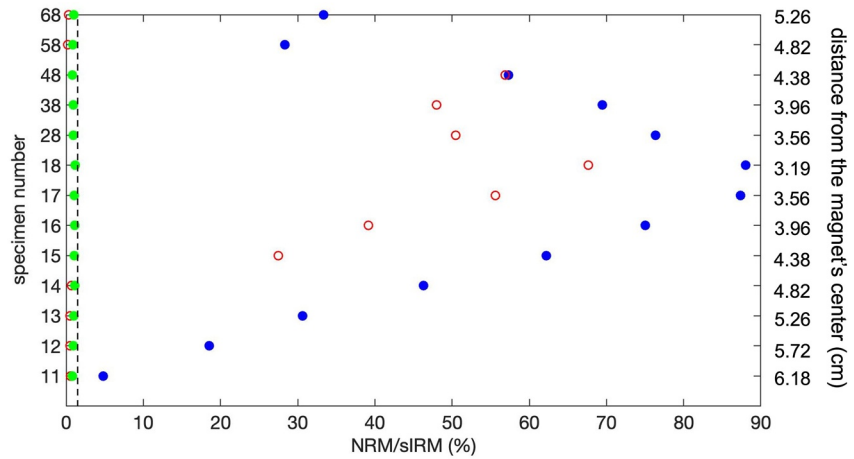


Figure 10. Proxies for the intensity of the magnetizing field of the basalt specimens. The REM value of the 13 basalt specimens after they have acquired an anhysteretic remanent magnetization (ARM) (green dots). The REM and integrated REM' value of the 13 basalt specimens after they have acquired an ARM and then were brought into proximity to a hand magnet (blue dots and red circles, respectively). The vertical black dashed line corresponds to 1.5%.

4. The Case of Martian Meteorite NWA 7034

We now turn our attention to the paleomagnetic record of actual meteorites. In particular we analyzed numerous pairs of the NWA 7034 group to assess whether any stones have been touched by magnets and, if not, to use them to study the ancient Martian magnetic field. Although Gattacceca and Rochette (2004) found that their samples of NWA 7034 and NWA 7533 were remagnetized by hand magnets, this still left at least nine members of the meteorite pairing group unmeasured. We were motivated to study these because in the occasion of a strewn field (i.e., the small region over which meteorite fragments scatter after the meteorite breaks up in Earth's atmosphere), it has been found that meteorite hunters sometimes use magnets only to identify the first few fragments until they become confident at identifying them visually (Weiss et al., 2017). With this in mind, we conducted an extensive search for samples of all paired stones of NWA 7034 in an effort to find any whose Martian magnetism has fortuitously survived arrival on Earth.

We analyzed the NRM of 11 specimens taken from NWA 7475, NWA 7906, NWA 7907, NWA 8114, NWA 11220, NWA 11896, NWA 11921, NWA 12222, and Rabt Sbayta (RS) 012 using a 2G Enterprises SRM equipped with an automated sample handler and demagnetization/remagnetization equipment (Kirschvink et al., 2008) in the Massachusetts Institute of Technology (MIT) Paleomagnetism Laboratory. To assess the effects of magnets on our samples, we followed the integrated REM' method (Gattacceca and Rochette, 2004; Weiss et al., 2008). We characterized the specimens' NRMs by using AF demagnetization with peak fields up to 420 mT. This value exceeds the peak coercivity of grains in the meteorite (300 mT), whose magnetization is dominated by magnetite in the pseudo-single domain (Gattacceca et al., 2014). This allowed us to identify the different components of the NRM for each specimen including the characteristic component. We then applied a sIRM (IRM of 400 mT) to the specimens and subjected them to the same step-wise demagnetization protocol as their NRMs in order to calculate the integrated REM' value. As discussed above, an integrated REM' value that is stronger than 1.5% by an order of magnitude or more signifies that the magnetization source is not of planetary origin and instead likely a hand magnet.

Figure 11a shows the histogram of the mass-normalized NRM values for all specimens and Figure 11b shows the histogram of the mass-normalized sIRM values for the 10 out of the 11 specimens (we did not measure the sIRM of NWA 11896 because of its large mass; see Table 1 for the masses of each specimen). We see that the NWA 7034 pairing group is quite magnetically homogeneous, with the sIRM values of the eight paired stones ranging from 1.65 to 2 Am²/kg. These NRM and sIRM values correspond to REM values between 37% and 95% for nine specimens; we could only estimate a lower limit of 12.05% for NWA 11896 because its NRM saturated the magnetometer (Figure 12). According to these REM estimates, all nine paired stones have been remagnetized since their arrival on Earth by strong hand magnets.

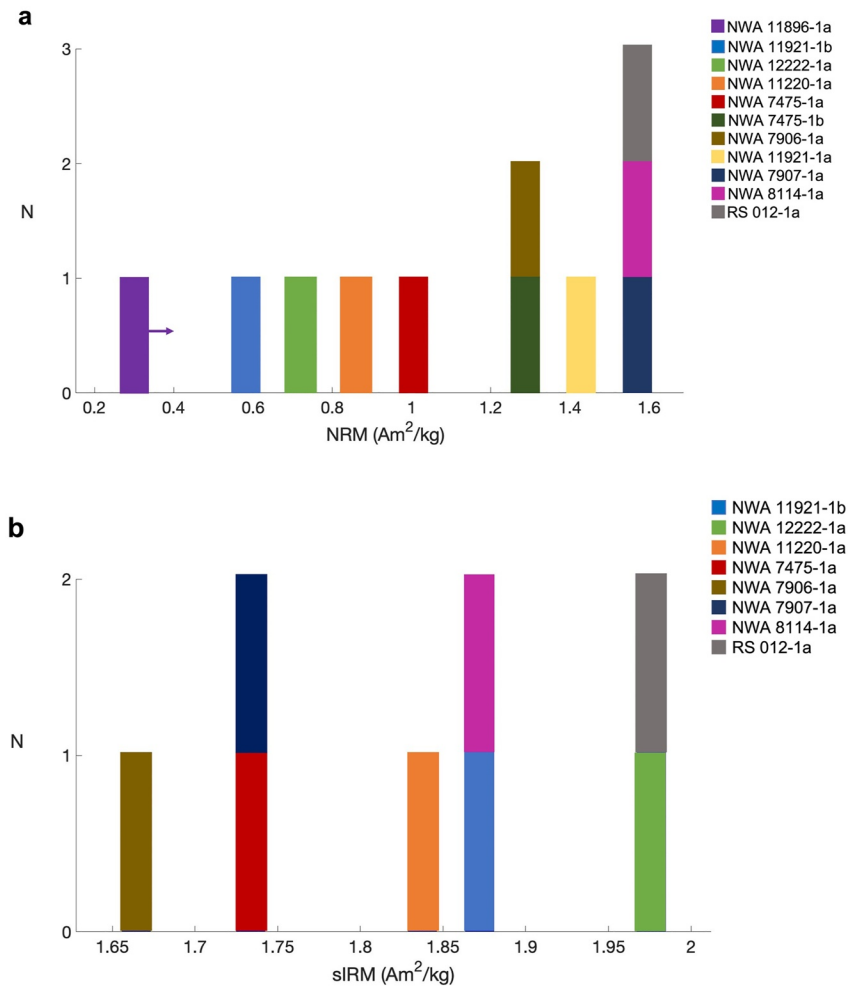


Figure 11. Histograms of the mass-normalized natural remanent magnetization (NRM) and saturation isothermal remanent magnetization (sIRM) for specimens from nine Northwest Africa (NWA) 7034 paired stones. NWA 11896, with a mass of 1.022 g, saturated the 2G and therefore the NRM value is only a lower limit. For the same reason, its sIRM was not measured. sIRM values were measured for one specimen per paired stone.

However, as demonstrated in Section 3, this still leaves open the possibility that they have only partially been remagnetized. To assess this, we also calculated the integrated REM' values. Table 1 presents a description of the characteristic component (AF range, direction, maximum angle of deviation, and deviation angle), along with the integrated REM' value and the specimen's mass, for all specimens. We found that for all specimens but one, the integrated REM' value is an order of magnitude larger than 1.5% and ranges from 15% to 109%. These specimens also exhibit smooth, curvilinear demagnetization trends that are a tell-tale sign of magnet remagnetization (see above). These results show that 10 out of the 11 specimens have apparently not retained any record of the magnetic field on Mars.

For one specimen of the 80-g stone NWA 7475 (specimen 1a), we found that the integrated REM' is equal to 1.67% over the AF range between 220 and 420 mT (using the mass-normalized sIRM demagnetization values of specimen NWA 11921). This integrated REM' value indicates that this specimen's magnetization may have not been completely overprinted. According to Figure 1, this specimen could have originated from the core of the NWA 7475 stone, where the maximum field of a typical 2 × 4 × 4 cm hand magnet with a 0.5 T surface field would have not exceeded 200 mT (see results for the 80-g rock in Figure 1a). The 1.67% ratio corresponds to the magnetization that would have been acquired during cooling on Mars in a field with paleointensity ≈50 μT. However, the remanence over this coercivity range is only 0.02% of the initial NRM and could still be partially contaminated, making the 50 μT an upper limit on the intensity of the Martian field.

Table 1

Properties of the Natural Remanent Magnetization (NRM) Characteristic Component of This Study's Specimens From Northwest Africa (NWA) 7034 Paired Stones

Specimen	Weight (mg)	Range (mT)	Nonanchored to the origin				Anchored to the origin			Integrated REM' (%)
			<i>D</i> (°)	<i>I</i> (°)	MAD (°)	DANG (°)	<i>D</i> (°)	<i>I</i> (°)	MAD (°)	
NWA 7475-1a ^a	5	220–420	242	−15.6	39	17.2	237.9	−0.7	17.6	1.67
NWA 7475-1b ^a	7.5	330–420	230.5	−37.3	19.8	12.6	226.3	−46.8	10.8	29.3
NWA 7906-1a	68	190–420	205.2	39	4.2	4.5				46.44
NWA 7907-1a	75	270–420	209.3	46.2	3.4	5.8				70.86
NWA 8114-1a	6.5	0–420	297	−57.1	1.1	0.6	296.8	−57.3	1	87.5
NWA 11220-1a ^a	20	80–400	358.1	38.7	1.1	1	357.5	38.6	1	53.31
NWA 11896-1a ^a	1,022	280–420	88.6	30.2	7.9	6.9	94.1	29.6	5.4	34.23
NWA 11921-1a	20	250–420	90.4	−76.2	2.2	9				94.25
NWA 11921-1b	13.5	350–420	260.5	−36.6	41	10.7	267.2	−28.7	18.1	15.37
NWA 12222-1a	10	210–420	174.2	29.3	3.1	3	173	30.4	2.6	60.05
RS 012-1a	15	150–420	41.1	−16.5	4.1	2.2	42.2	−16.5	3.2	109.3

Note. NRM characteristic component obtained using alternating field demagnetization (up to 400 mT for NWA 11220 and 420 mT for all the others). Declination (*D*), inclination (*I*), maximum angular deviation (MAD) and deviation angle (DANG) estimated from principal component analysis. See text for details on the calculation of integrated REM'.

^aThe integrated REM' value has been calculated using the saturation isothermal remanent magnetization demagnetization values of specimen NWA 11921-1a.

The second smallest integrated REM' is 15%, which we measured for NWA 11921-1b, a specimen obtained from the core of a 5.95 g NWA 11921 stone. Specimen NWA 11921-1a, which was obtained from the surface of the same rock, gives integrated REM' equal to 53%. According to Figure 1, the near-total remagnetization of the center of NWA 11921 can also be explained by the use of a 2 × 4 × 4 cm hand magnet with a 0.5 T surface field, which would have produced fields up to 300 mT at this location (see results for the 6-g rock in Figure 1a).

The NRM demagnetization curves of specimens NWA 7475-1a and NWA 11921-1b are shown in Figures 13a and 13b. We see that the characteristic components of these two specimens, shown in the inset of Figures 13a and 13b, are less curvilinear and are noisier than the low-AF field parts of the respective demagnetization curves. For comparison, the NRM demagnetization curve of specimen NWA 8114-1a, with an integrated REM' value of 87.5%, is shown in Figure 13c. We see that it is characterized by a single, origin-trending component over

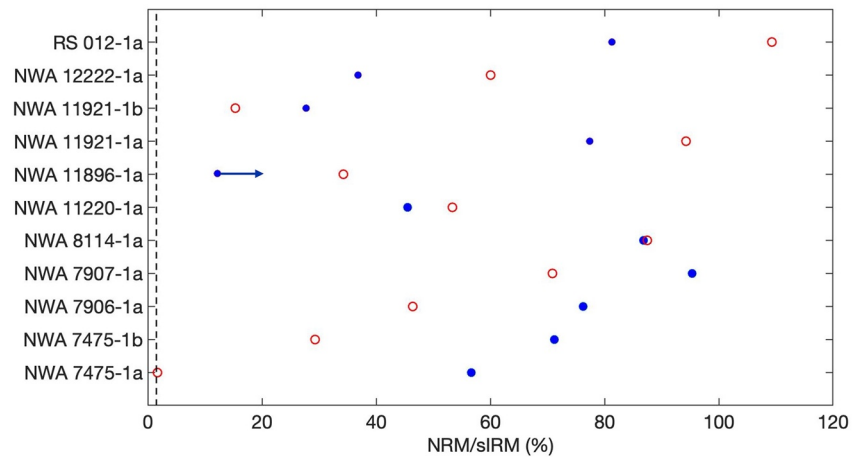


Figure 12. The ratio of natural remanent magnetization to sIRM for specimens from nine Northwest Africa (NWA) 7034 paired stones. Blue dots correspond to REM values and red open circles correspond to integrated REM' values. The REM value of NWA 11896 is a lower limit. See Table 1 for the integrated REM' values and the properties of the characteristic component over which these were estimated. The vertical dashed line marks the value 1.5%.

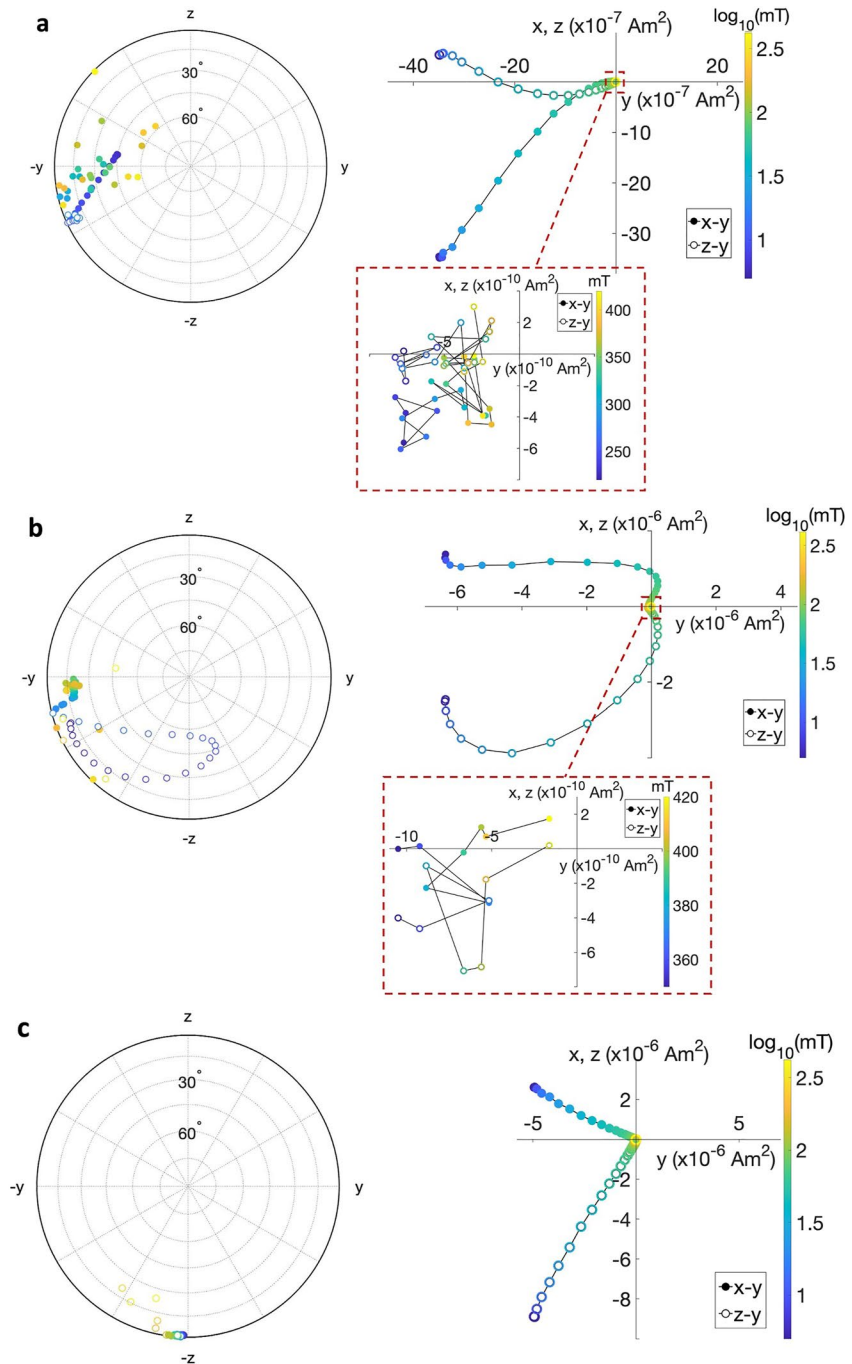


Figure 13. Natural remanent magnetization (NRM) demagnetization of three paired stones of the ancient Martian meteorite Northwest Africa (NWA) 7034. Shown are endpoints of the NRM vectors during progressive alternating field (AF) demagnetization. Closed and open symbols on the stereoplots correspond to endpoints on the lower ($x < 0$) and upper hemisphere ($x > 0$), respectively. Closed and open symbols on the orthographic plots correspond to projections of the NRM vectors onto the y - x and y - z planes, respectively. The coordinate system relates to the specimens' orientation and not to actual Martian geographic coordinates. (a) Specimen NWA 7475-1a. Inset: AF demagnetization steps from 220 to 420 mT. (b) Specimen NWA 11921-1b. Inset: AF demagnetization steps from 350 to 420 mT. (c) Specimen NWA 8114-1a.

the entire range of 0–420 mT. Figures S2 and S3 in Supporting Information S1 show the NRM demagnetization curves of the other eight specimens, over the entire AF range and over the range of their characteristic component. In agreement with the conclusions of Section 3, most of these NRMs are multi-component and/or curvilinear. Figure S4 in Supporting Information S1 shows the NRM lost as a function of sIRM lost during AF

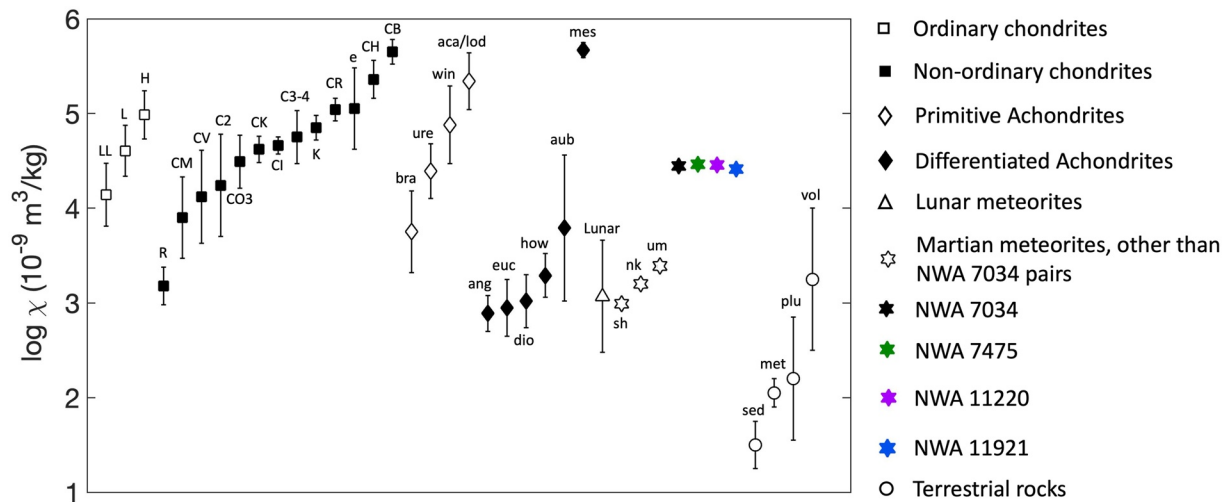


Figure 14. The decimal logarithm of magnetic susceptibility for different groups of meteorites and some terrestrial rock types. Shown are the mean values and standard deviations. The values for Northwest Africa (NWA) 7475, NWA 11220, and NWA 11921 were obtained by this study, while all other values were obtained from the literature. “e” stands for enstatites, “bra” for brachinites, “ure” for ureilites, “win” for winonaites, “aca/lod” for acapulcoites/londranites, “ang” for Angrites, “euc” for eucrites, “dio” for diogenites, “how” for howardites, “aub” for aubrites, “mes” for mesosiderites, “sh” for basaltic shergottites, “nk” for nakhlites, “um” for Martian ultramafics (i.e., ALH A77005, ALH 84001, Chassigny, and LEW 88516), and “sed,” “met,” “plu,” and “vol” for sedimentary, metamorphic, plutonic, and volcanic Earth rocks, respectively. See Table S2 in Supporting Information S1 for the exact values and the respective references.

demagnetization for specimen NWA 8114, whose NRM had only one component (see Figure 13c), and specimen RS 012, whose NRM had two components (see Figure S3 in Supporting Information S1). For both these specimens, this paleointensity slope is very close to 1, in agreement with the high integrated REM’ values obtained for both of them (87.5% and 109.3%).

5. An Alternative Meteorite Identification Technique

The use of magnetic susceptibility meters has been shown by many studies to be an accurate and nondestructive meteorite identification and classification technique (Folco et al., 2006; Kohout et al., 2010; Macke, 2010). They can be used to not only distinguish between meteorites and terrestrial rocks (identification) but also to distinguish among different types of meteorites (classification). Rochette et al. (2003), Rochette et al. (2005, 2008, 2009, 2010) have compiled an extensive database with magnetic susceptibility values for different meteorite types, including Martian and lunar rocks. Indicative of the simplicity and efficiency of magnetic susceptibility measurements for meteorite identification and classification, it has been suggested they are suitable for automated execution by robots, rovers, and landers, facilitating meteorite collection and sample return missions, on Earth, other planets, and asteroids (Folco et al., 2006; Kohout & Britt, 2011).

There is a large variety of susceptibility meters, including portable pocket-sized instruments. Gattaceca et al. (2004) describe a simple protocol that enables the calibration of such a handheld instrument for in situ magnetic susceptibility measurements. Folco et al. (2006) applied this protocol for in situ identification, pairing and classification of meteorites during an expedition in Antarctica within the framework of the Italian Antarctic Research Project (Programma Nazionale di Ricerche in Antartide or PNRA). Further applications of this protocol include the work by ElkShoulder et al. (2006) and Macke (2010).

In Figure 14, we summarize low-field magnetic susceptibility values for different groups of meteorites and main terrestrial rock types, as obtained from the available literature (see Table S2 in Supporting Information S1 for the respective references). We also include the values we measured from specimens of three NWA 7034 paired stones, using an AGICO KLY-3-CS3 Kappabridge susceptibility meter: NWA 7475-1c (243 mg), NWA 11220-1a (20 mg), and NWA 11921-1c (36.5 mg), shown in green, purple, and blue stars, respectively. We see that most Martian and lunar meteorites have magnetic susceptibilities in the same range as other achondrites and in terms of terrestrial rocks only overlap with some basalts. However, NWA 7034 and paired stones have magnetic susceptibilities that are an order of magnitude stronger, overlapping only with chondrites and some primitive

achondrites. All four stones of the NWA 7034 pairing group gave essentially the same magnetic susceptibility values.

6. Conclusions

Meteorites carry unique information concerning the geological history of other planetary bodies. While touching or approaching a meteorite with a hand magnet is inconsequential for many kinds of analytical studies (e.g., petrography and elemental and isotopic composition), it is irreversibly detrimental to the paleomagnetic record of the meteorite. We therefore recommend that meteorites never be touched or approached with magnets.

Here, we showed by means of numerical calculations, a controlled remagnetization experiment on a terrestrial basalt and a paleomagnetic study of nine paired stones of Martian meteorite NWA 7034, the typical characteristics of rocks exposed to hand magnets:

1. The integrated REM' value is at least one order of magnitude larger than 1.5%.
2. The intensity of the acquired magnetization increases from inside of the meteorite outward.
3. The orientation of the acquired magnetization varies across the rock sample.
4. The magnetization of individual specimens is often multicomponent and/or its demagnetization pattern is curvilinear.

Another possible test to discuss here is to conduct a fusion crust test. As meteoroids enter the Earth's atmosphere, they heat to the point they melt. The remaining mass forms a thin black glassy surface layer that remains visible until it weathers away. For meteorites that have still at least part of their fusion crust intact, the fusion crust test consists in comparing the magnetization direction of the fusion crust with that of the interior (Borlina et al., 2022; Weiss et al., 2010). If they are the same, this suggests that the rock sample has been remagnetized since its landing on Earth.

A better identification technique than the use of magnets is to use magnetic susceptibility meters because they are nondestructive due to their weak fields (<0.5 mT), quantitative, and can more sensitively distinguish between meteorite groups including identifying rare meteorites like those from Mars and the Moon that are poor in iron (Folco et al., 2006).

We remain hopeful that more paired stones of NWA 7034 and new Martian meteorite finds will become available in the near future that are free of the effects of magnet remagnetization. Otherwise, we anticipate future magnetic studies of rock samples from Mars on the cores currently being collected at Jezero crater by the Perseverance rover (Mangold et al., 2021; Mittelholz et al., 2018), expected to be delivered to Earth in the early 2030s. We advocate that the Mars sample return campaign not expose these samples to fields larger than several mT during the entire process from sampling to return to Earth (Beaty et al., 2019).

Data Availability Statement

The paleomagnetic data of the NWA 7034 paired stones of this study have been uploaded to the Magnetism Information Consortium (MagIC) database (Vervelidou et al., 2023).

References

- Agee, C. B., Wilson, N. V., McCubbin, F. M., Ziegler, K., Polyak, V. J., Sharp, Z. D., et al. (2013). Unique meteorite from early Amazonian Mars: Water-rich basaltic breccia Northwest Africa 7034. *Science*, 339(6121), 780–785. <https://doi.org/10.1126/science.1228858>
- Beaty, D. W., Grady, M. M., McSween, H. Y., Sefton-Nash, E., Carrier, B. L., Altieri, F., et al. (2019). The potential science and engineering value of samples delivered to Earth by Mars sample return: International MSR Objectives and Samples Team (iMOST). *Meteoritics & Planetary Science*, 54(S1), S3–S152. <https://doi.org/10.1111/maps.13242>
- Bischoff, A., Alexander, C. M. D., Barrat, J. A., Burkhardt, C., Busemann, H., Degering, D., et al. (2021). The old, unique C1 chondrite Flensburg—Insight into the first processes of aqueous alteration, brecciation, and the diversity of water-bearing parent bodies and lithologies. *Geochimica et Cosmochimica Acta*, 293, 142–186. <https://doi.org/10.1016/j.gca.2020.10.014>
- Borlina, C. S., Weiss, B. P., Bryson, J. F., & Armitage, P. J. (2022). Lifetime of the outer solar system nebula from carbonaceous chondrites. *Journal of Geophysical Research*, 127(7), e2021JE007139. <https://doi.org/10.1029/2021je007139>
- Bouvier, L. C., Costa, M. M., Connelly, J. N., Jensen, N. K., Wielandt, D., Storey, M., et al. (2018). Evidence for extremely rapid magma ocean crystallization and crust formation on Mars. *Nature*, 558(7711), 586–589. <https://doi.org/10.1038/s41586-018-0222-z>
- Camacho, J. M., & Sosa, V. (2013). Alternative method to calculate the magnetic field of permanent magnets with azimuthal symmetry. *Revista Mexicana de Física E*, 59(1), 8–17.

Acknowledgments

We wish to thank the Smithsonian Institution, Washington, D.C., US for a loan of NWA 11896, Addi Bischoff, Institut für Planetologie, Münster, Germany for a loan of NWA 12222, Beda Hofmann, Natural History Museum Bern, Switzerland, for a loan of NWA 7906 and NWA 7907, Alan Rubin, UCLA, USA, for a loan of RS012, John Bridges, University of Leicester, UK for a loan of NWA 8114, Said Yousfi for kindly offering to cut a rock of NWA 11921 in slices and let us choose the innermost piece of the middle slice for our measurements, Julie Carlut for providing us with the terrestrial basalt sample, and Eduardo Andrade Lima, Jay Shah, and Adriana Gonzalez for assistance with the operation and maintenance of the instrumentation. This project has received funding from the European Union's Horizon 2020 research and innovation programme under the Marie Skłodowska-Curie grant agreement No 844252. One specimen of NWA 11220 was purchased by Martin Goff, two specimens of NWA 7475 were purchased by Luc Labenne, and two specimens of NWA 11921 were purchased by Said Yousfi, with funds from the latter programme. F.V. and B.P.W. also acknowledge the NASA Mars 2020 Returned Sample Scientist Participating Scientist Grant 80NSSC20K0238 for funding. The manuscript has greatly benefited from the reviews and recommendations by Jérôme Gattacceca, an anonymous reviewer, an anonymous associate editor of the journal, and the editor Laurent Montési.

- Cassata, W. S., Cohen, B. E., Mark, D. F., Trappitsch, R., Crow, C. A., Wimpenny, J., et al. (2018). Chronology of martian breccia NWA 7034 and the formation of the martian crustal dichotomy. *Science Advances*, 4(5), eaap8306. <https://doi.org/10.1126/sciadv.aap8306>
- Cébron, D. (2021). Magnetic fields of solenoids and magnets, MATLAB Central File Exchange. Retrieved from <https://www.mathworks.com/matlabcentral/fileexchange/71881-magnetic-fields-of-solenoids-and-magnets>
- ElkShoulder, A., Franklin, J., Yawea, O., Gchachu, K., Simmons, J., Cohen, B. A., & Newsom, H. E. (2006). Meteorite identification and classification using magnetic susceptibility. In *Lunar and Planetary Science Conference XXXVII*, abstract #1485.
- Folco, L., Rochette, P., Gattacceca, J., & Perchiazzi, N. (2006). In situ identification, pairing, and classification of meteorites from Antarctica through magnetic susceptibility measurements. *Meteoritics & Planetary Science*, 41(3), 343–353. <https://doi.org/10.1111/j.1945-5100.2006.tb00467.x>
- Gattacceca, J., Eisenlohr, P., & Rochette, P. (2004). Calibration of *in situ* magnetic susceptibility measurements. *Geophysical Journal International*, 158(1), 42–49. <https://doi.org/10.1111/j.1365-246x.2004.02297.x>
- Gattacceca, J., & Rochette, P. (2004). Toward a robust normalized magnetic paleointensity method applied to meteorites. *Earth and Planetary Science Letters*, 227(3–4), 377–393. <https://doi.org/10.1016/j.epsl.2004.09.013>
- Gattacceca, J., Rochette, P., Scorzelli, R. B., Munayco, P., Agee, C., Quesnel, Y., et al. (2014). Martian meteorites and Martian magnetic anomalies: A new perspective from NWA 7034. *Geophysical Research Letters*, 41(14), 4859–4864. <https://doi.org/10.1002/2014gl060464>
- Harvey, R. P., Schutt, J., & Karner, J. (2014). Fieldwork methods of the U.S. Antarctic Search for Meteorites Program. In K. Righter, C. M. Corrigan, T. J. McCoy, & R. P. Harvey (Eds.), *35 seasons of U.S. Antarctic meteorites (1976–2010): A pictorial guide to the collection* (pp. 23–41). American Geophysical Union.
- Johnson, C. L., Mittelholz, A., Langlais, B., Russell, C. T., Ansan, V., Banfield, D., et al. (2020). Crustal and time-varying magnetic fields at the InSight landing site on Mars. *Nature Geoscience*, 13(3), 199–204. <https://doi.org/10.1038/s41561-020-0537-x>
- Kirschvink, J. L., Kopp, R. E., Raub, T. D., Baumgartner, C. T., & Holt, J. W. (2008). Rapid, precise, and high-sensitivity acquisition of paleomagnetic and rock-magnetic data: Development of a low-noise automatic sample changing system for superconducting rock magnetometers. *Geochemistry, Geophysics, Geosystems*, 9(5), Q05Y01. <https://doi.org/10.1029/2007GC001856>
- K & J Magnetics, Inc. (2023). Pull force and surface field data. Retrieved from <https://www.kjmagnetics.com/magnetsummary.asp>
- Kletetschka, G., Kohout, T., & Wasilewski, P. J. (2003). Magnetic remanence in the Murchison meteorite. *Meteoritics & Planetary Science*, 38(3), 399–405. <https://doi.org/10.1111/j.1945-5100.2003.tb00275.x>
- Kohout, T., & Britt, D. (2011). Magnetic susceptibility as a tool for characterization of an asteroid regolith and sample return. In *EPSC abstracts. EPSC-DPS Joint Meeting 2011, EPSC-DPS2011-784* (Vol. 6).
- Kohout, T., Jenniskens, P., Shaddad, M. H., & Haloda, J. (2010). Inhomogeneity of asteroid 2008 TC₃ (Almahata Sitta meteorites) revealed through magnetic susceptibility measurements. *Meteoritics & Planetary Science*, 45(10–11), 1778–1788. <https://doi.org/10.1111/j.1945-5100.2010.01110.x>
- Langlais, B., Thébaud, E., Houliéz, A., Purucker, M. E., & Lillis, R. J. (2019). A new model of the crustal magnetic field of Mars using MGS and MAVEN. *Journal of Geophysical Research*, 124(6), 1542–1569. <https://doi.org/10.1029/2018je005854>
- Love, S. G. (2013). *The Antarctic search for meteorites: A model for deep space exploration (technical report no. NASA/TM-2014-217388)*. NASA Johnson Space Center.
- Lundin, R., Lammer, H., & Ribas, I. (2007). Planetary magnetic fields and solar forcing: Implications for atmospheric evolution. *Space Science Reviews*, 129, 245–278. <https://doi.org/10.1007/s11214-007-9176-4>
- Macke, R. J. (2010). *Survey of meteorite physical properties density, porosity and magnetic susceptibility* (Doctoral dissertation). University of Central Florida. Retrieved from <https://stars.library.ucf.edu/etd/1638>
- Mangold, N., Gupta, S., Gasnault, O., Dromart, G., Tarnas, J. D., Sholes, S. F., et al. (2021). Perseverance rover reveals an ancient delta-lake system and flood deposits at Jezero crater, Mars. *Science*, 374(6568), 711–717. <https://doi.org/10.1126/science.aba4051>
- McCubbin, F. M., Boyce, J. W., Novák-Szabó, T., Santos, A. R., Tartèse, R., Muttik, N., et al. (2016). Geologic history of Martian regolith breccia Northwest Africa 7034: Evidence for hydrothermal activity and lithologic diversity in the Martian crust. *Journal of Geophysical Research*, 121(10), 2120–2149. <https://doi.org/10.1002/2016je005143>
- MeteoriteMen (2022). What kind of magnets do you use? Retrieved from <https://www.meteoritemen.com/faq>
- Mittelholz, A., Johnson, C. L., Feinberg, J. M., Langlais, B., & Phillips, R. J. (2020). Timing of the martian dynamo: New constraints for a core field 4.5 and 3.7 Ga ago. *Science Advances*, 6(18), eaba0513. <https://doi.org/10.1126/sciadv.aba0513>
- Mittelholz, A., Morschhauser, A., Johnson, C. L., Langlais, B., Lillis, R. J., Vervelidou, F., & Weiss, B. P. (2018). The Mars 2020 candidate landing sites: A magnetic field perspective. *Earth and Space Science*, 5(9), 410–424. <https://doi.org/10.1029/2018ea000420>
- Morschhauser, A., Vervelidou, F., Thomas, P., Grott, M., Lesur, V., & Gilder, S. A. (2018). Mars' Crustal Magnetic Field. In H. Lühr, J. Wicht, S. A. Gilder, & M. Holschneider (Eds.), *Magnetic Fields in the Solar System* (Vol. 448, pp. 331–356). Astrophysics and Space Science Library. Springer. https://doi.org/10.1007/978-3-319-64292-5_12
- Nyquist, L. E., Bogard, D. D., Shih, C. Y., Greshake, A., Stöfler, D., & Eugster, O. (2001). Ages and geologic histories of Martian meteorites. In *Chronology and Evolution of Mars: Proceedings of an ISSI Workshop, 10–14 April 2000, Bern, Switzerland* (pp. 105–164). Springer Netherlands.
- Ricci, J., Carlut, J., Marques, F. O., Hildenbrand, A., & Valet, J. P. (2020). Volcanic record of the last geomagnetic reversal in a lava flow sequence from the Azores. *Frontiers in Earth Science*, 8, 165. <https://doi.org/10.3389/feart.2020.00165>
- Rochette, P., Gattacceca, J., Bonal, L., Bourrot-Denise, M., Chevrier, V., Clerc, J. P., et al. (2008). Magnetic classification of stony meteorites: 2. Non-ordinary chondrites. *Meteoritics & Planetary Science*, 43(5), 959–980. <https://doi.org/10.1111/j.1945-5100.2008.tb01092.x>
- Rochette, P., Gattacceca, J., Bourrot-Denise, M., Consolmagno, G., Folco, L., Kohout, T., et al. (2009). Magnetic classification of stony meteorites: 3. Achondrites. *Meteoritics & Planetary Science*, 44(3), 405–427. <https://doi.org/10.1111/j.1945-5100.2009.tb00741.x>
- Rochette, P., Gattacceca, J., Chevrier, V., Hoffmann, V., Lorand, J. P., Funaki, M., & Hochleitner, R. (2005). Matching Martian crustal magnetization and magnetic properties of Martian meteorites. *Meteoritics & Planetary Sciences*, 40(4), 529–540. <https://doi.org/10.1111/j.1945-5100.2005.tb00961.x>
- Rochette, P., Gattacceca, J., Ivanov, A. V., Nazarov, M. A., & Bezaeva, N. S. (2010). Magnetic properties of lunar materials: Meteorites, Luna and Apollo returned samples. *Earth and Planetary Science Letters*, 292(3–4), 383–391. <https://doi.org/10.1016/j.epsl.2010.02.007>
- Rochette, P., Lorand, J. P., Fillion, G., & Sautter, V. (2001). Pyrrhotite and the remanent magnetization of SNC meteorites: A changing perspective on Martian magnetism. *Earth and Planetary Science Letters*, 190(1–2), 1–12. [https://doi.org/10.1016/s0012-821x\(01\)00373-9](https://doi.org/10.1016/s0012-821x(01)00373-9)
- Rochette, P., Sagnotti, L., Bourrot-Denise, M., Consolmagno, G., Folco, L., Gattacceca, J., et al. (2003). Magnetic classification of stony meteorites: 1. Ordinary chondrites. *Meteoritics & Planetary Science*, 38(2), 251–268. <https://doi.org/10.1111/j.1945-5100.2003.tb00263.x>
- Sakata, R., Seki, K., Sakai, S., Terada, N., Shinagawa, H., & Tanaka, T. (2020). Effects of an intrinsic magnetic field on ion loss from ancient Mars based on multispecies MHD simulations. *Journal of Geophysical Research*, 125(2), e2019JA026945. <https://doi.org/10.1029/2019JA026945>

- Udry, A., Howarth, G. H., Herd, C. D. K., Day, J. M. D., Lapen, T. J., & Filiberto, J. (2020). What Martian meteorites reveal about the interior and surface of Mars. *Journal of Geophysical Research*, *125*(12), e2020JE006523. <https://doi.org/10.1029/2020JE006523>
- Vervelidou, F., Weiss, B. P., & Lagroix, F. (2023). Hand magnets and the destruction of ancient meteorite magnetism [Dataset]. Magnetics Information Consortium (MagIC). <https://doi.org/10.7288/V4/MAGIC/19658>
- Wasilewski, P., & Dickinson, T. (2000). Aspects of the validation of magnetic remanence in meteorites. *Meteoritics & Planetary Science*, *35*(3), 537–544. <https://doi.org/10.1111/j.1945-5100.2000.tb01434.x>
- Weir, G. J., Chisholm, G., & Leveneur, J. (2020). The magnetic field about a three-dimensional block neodymium magnet. *The ANZIAM Journal*, *62*(4), 386–405. <https://doi.org/10.21914/anziamj.v62.14220>
- Weisberg, M. K., McCoy, T. J., & Krot, A. N. (2006). Systematics and evaluation of meteorite classification. In D. S. Lauretta & H. Y. McSween (Eds.), *Meteorites and the early solar system II* (pp. 19–52). University of Arizona Press.
- Weiss, B. P., & Elkins-Tanton, L. (2013). Differentiated planetesimals and the parent bodies of chondrites. *Annual Review of Earth and Planetary Sciences*, *41*, 529–560. <https://doi.org/10.1146/annurev-earth-040610-133520>
- Weiss, B. P., Fong, L. E., Vali, H., Lima, E. A., & Baudenbacher, F. J. (2008). Paleointensity of the ancient Martian magnetic field. *Geophysical Research Letters*, *35*(23), L23207. <https://doi.org/10.1029/2008GL035585>
- Weiss, B. P., Gattacceca, J., Stanley, S., Rochette, P., & Christensen, U. R. (2010). Paleomagnetic records of meteorites and early planetesimal differentiation. *Space Science Reviews*, *152*, 341–390. <https://doi.org/10.1007/s11214-009-9580-z>
- Weiss, B. P., Wang, H., Sharp, T. G., Gattacceca, J., Shuster, D. L., Downey, B., et al. (2017). A nonmagnetic differentiated early planetary body. *Earth and Planetary Science Letters*, *468*, 119–132. <https://doi.org/10.1016/j.epsl.2017.03.026>
- Yang, Z. J., Johansen, T. H., Bratsberg, H., Helgesen, G., & Skjeltorp, A. T. (1990). Potential and force between a magnet and a bulk $Y_1Ba_2Cu_3O_{7-\delta}$ superconductor studied by a mechanical pendulum. *Superconductor Science and Technology*, *3*(12), 591–597. <https://doi.org/10.1088/0953-2048/3/12/004>
- Yu, Y., Dunlop, D. J., & Özdemir, Ö. (2003). Are ARM and TRM analogs? Thellier analysis of ARM and pseudo-Thellier analysis of TRM. *Earth and Planetary Science Letters*, *205*(3–4), 325–336. [https://doi.org/10.1016/s0012-821x\(02\)01060-9](https://doi.org/10.1016/s0012-821x(02)01060-9)